

Low-noise CMOS Fluorescence Sensor

David Sander, Marc Dandin, Honghao Ji, Nicole Nelson, Pamela Abshire
Department of Electrical and Computer Engineering Institute for Systems Research
University of Maryland, College Park, Maryland 20742 USA
Email: {dsander, mpdandin, jhonghao, nmnelson, pabshire}@umd.edu

Abstract—This paper reports a novel integrated circuit for fluorescence sensing. The circuit implements a differential readout architecture in order to reduce the overall noise figure. The circuit has been fabricated in a commercially available $0.5\ \mu\text{m}$ CMOS technology. Preliminary results show that the reset noise is reduced by a factor of 1.42 and the readout noise by a factor of 9.20 when the pixel is operated in differential mode versus single-ended mode. Spectral responsivity characteristics show that the photodiodes are most sensitive at 480 nm. Using a commercially available emission filter, the sensor was able to reliably detect a concentration of Fura-2 as low as 39 nM. The sensor was used to perform ratiometric measurements and was able to reliably detect a free calcium concentration of 17 nM.

I. INTRODUCTION

Fluorescence sensing is a mature technology commonly used in cell biology. For many analytes it provides the highest sensitivity and selectivity available. The ability to detect fluorescence on-chip is an important feature of lab-on-a-chip devices. Several groups [1]–[5] are pursuing integrated fluorescence sensing for applications ranging from DNA analysis to pathogen detection. The devices demonstrated in these works make use of conventional detector architectures (reverse biased p-n and p-i-n junctions) for transduction of fluorescence. However, achieving high-sensitivity fluorescence detection requires high quality optical filters as well as high quality optical detectors. In particular, detector noise must be reduced below the signal level to be detected (usually less than $10\ \text{photons}/\mu\text{m}^2\cdot\text{s}$).

In this paper, we propose an active pixel sensor architecture in which the photocurrent is measured differentially. Experimental results demonstrate that reset and readout noise are both reduced when the pixel is operated in this manner. The detector is a p+/nwell junction which offers high sensitivity in the blue to green region of the electromagnetic spectrum. This makes the sensor ideal for use in a wide range of fluorescence assays, one example of which is monitoring calcium levels using the fluorophore Fura-2. The following sections describe the operation of the sensor and present results of a preliminary analysis on noise reduction in differential mode operation. We then present measurements and characterization of the spectral responsivity of the detector along with demonstration of fluorescence collection using an external macroscopic emission filter.

II. SENSOR OPERATION AND NOISE ANALYSIS

The detector is a 6-transistor differential active pixel sensor with in-pixel sampling of the reset voltage (Figure 1). The reset

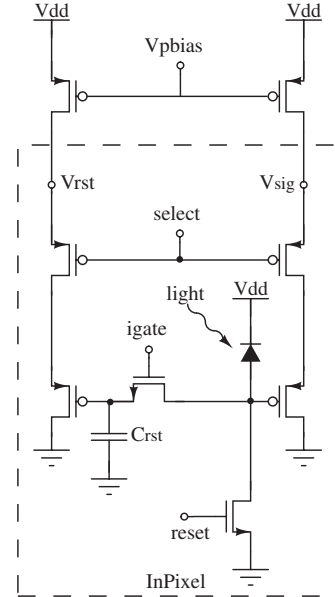


Fig. 1. Differential pixel schematic

voltage is held on a capacitor and read out alongside the signal at the end of the integration period. By sampling the reset voltage and reading out the signal differentially it is possible in principle to virtually eliminate reset noise. Power supply noise and other coupled noise sources will also be suppressed substantially. In practice the suppression of reset noise and readout noise will be limited by charge injection and coupling.

The optically active area is a $33.6\ \mu\text{m} \times 33.6\ \mu\text{m}$ p+/nwell reverse biased diode where the nwell is tied to the power supply Vdd. The p+/nwell junction helps to reduce noise by decoupling the sensor from the substrate as well as suppressing blooming effects. The hold capacitor is not required to be linear so it can be implemented with a MOSCAP or other nonlinear capacitance. In this circuit it has been implemented as a linear poly-poly capacitor for convenience, with nominal value of 20 fF.

To examine the benefits of a differential readout with in-pixel sample and hold, we compare measurements from the sensor in single-ended mode to those in differential mode. In single-ended mode, the i_gate transistor is off for the entire experiment, and the output of the sensor is measured with respect to ground. Reset and select signals initialize the pixel before integration and select a row of pixels for readout after

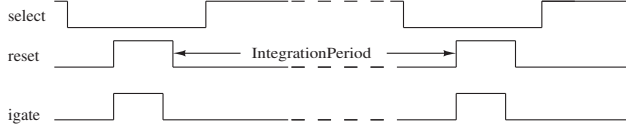


Fig. 2. Timing diagram for differential sensor

integration as in a standard APS.

For differential mode, three control signals are required to operate the pixel: select, reset, and i_gate (isolation gate). The isolation gate is on during the reset cycle and turns off immediately before the end of the reset cycle. This minimizes noise due to charge injection by providing a low impedance node for dissipation of channel charges when both the isolation gate and reset gate close. Figure 2 shows the timing diagram.

A series of 50 integration paths were measured for the sensor in single ended and differential mode of operation over 3 orders magnitude of incident illumination. The illumination source was controlled using a monochromator and integrating sphere. The wavelength was 630 nm with 20 nm spread and output power fixed at 95.2 nW/mm^2 . A set of neutral density filters were used to decrease the optical power at the output of the integrating sphere. The neutral density filters were varied from optical density (OD) 2 to OD 5 in 0.5 increments. We chose 630 nm because the neutral density filters are well characterized for 630 nm light.

The total variance of the measured reset voltage is the sum of reset noise and readout noise. Using our estimated readout noise, and the measured reset noise, we can estimate the true reset noise.

$$\text{Var}[V_0] = \sigma_{readout}^2 + \sigma_{reset}^2 \quad (1)$$

Readout noise was estimated as described below, using the method outlined by Fowler [6]. The output voltage between two successive measurements is equal to:

$$V(i) = gQ_i + V_{noise}(i) - V_{noise}(S_1) \quad (2)$$

where g is the front end gain of the sensor, Q_i is the accumulated charge due to photocurrent and dark current, and V_{noise} is the reset and readout noise at samples (S_1) and i respectively. By subtracting successive measurements reset noise is eliminated and we are left with an output which is a function only of the photo-process and of the readout noise.

Considered as stochastic processes, the photocurrent and dark current are Poisson processes, while the readout and reset noise are assumed to be zero mean Gaussian processes. The mean and standard deviation between successive samples are given by:

$$E[V(i)] = g(I_{ph} + I_{dc})i\tau \quad (3)$$

$$\text{Var}[V(i)] = g^2(I_{ph} + I_{dc})i\tau + 2\sigma_{readout}^2 \quad (4)$$

where I_{ph} is the photocurrent, I_{dc} is the dark current, g is the sensor gain, i is the sample number, τ is the time interval

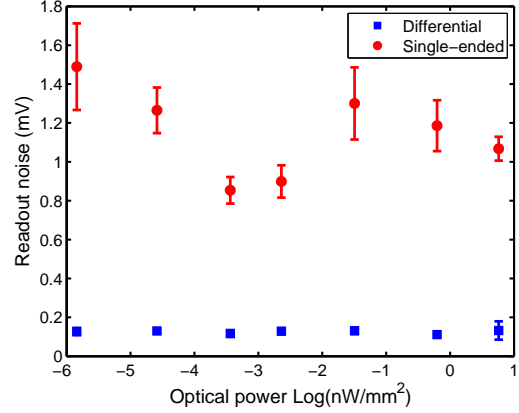


Fig. 3. Readout noise vs. optical power

between samples, and $\sigma_{readout}^2$ is the variance of the readout noise.

The measured integration paths are not strictly linear due to the nonlinear capacitance of the photodiode and other effects, so we select short segments that closely approximate linear paths from the overall integration path. We then find the linear least-square solution that best fits readout noise and shot noise across the same segment in all sample paths of the same illumination. Figure 3 shows the estimated readout noise under different illumination levels. Error bars are plotted for all data, but in some cases are too small to be visible. Under all illumination levels the estimated differential readout noise is consistently lower than the estimated single-ended readout noise.

Figure 4 shows the overall noise as a function of time for a pair of single ended and differential measurements taken at 4.4 nW/mm^2 (OD 3). These results were both computed by averaging 50 sample paths, and computing the standard deviation at each time step about the average value for that time step. The measurements exhibit noise that is transiently high, then decreases before beginning to rise again. This occurs for both the single ended and differential measurements but is more pronounced in the differential measurement. This transient is due to charge injection and clock feedthrough. As a result we take the noise after reset to be the average noise in the trough. After determining the noise after reset, we remove the estimated readout noise yielding the estimated reset noise.

Figure 5 shows the estimated reset noise under different illumination levels. Again, error bars are plotted for all data, but in some cases are too small to be visible. From the data in Figures 3 and 5, the sensor shows average reset noise improved by a factor of 1.42 ± 0.89 and average readout noise improved by a factor of 9.20 ± 1.78 in differential mode over single-ended mode.

III. SPECTRAL RESPONSIVITY

The spectral responsivity of the low-noise differential sensor was characterized in order to determine the range of excitation and emission wavelengths that the device can accommodate.

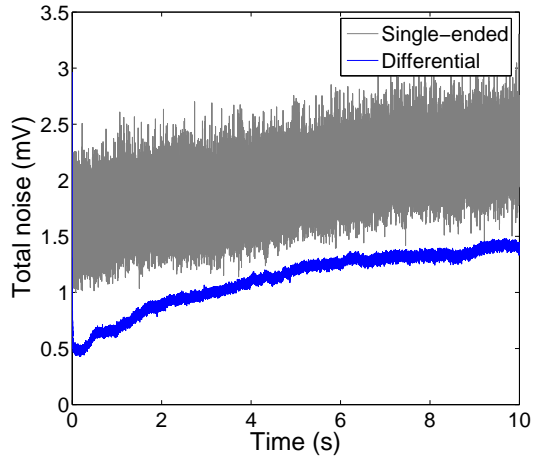


Fig. 4. Standard deviation noise path for 4.4 nW/mm² Illumination

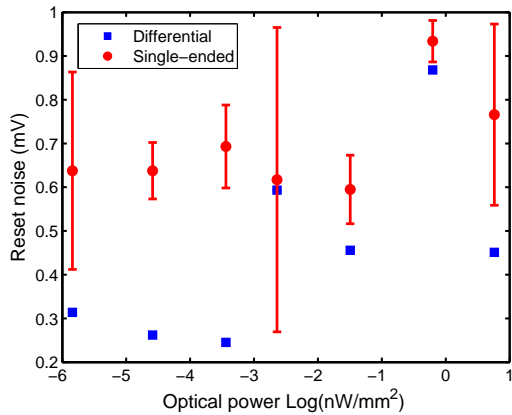


Fig. 5. Reset noise vs. optical power

For consistency, the spectral responsivity of the detector was also determined when operated in single-ended mode.

A grating monochromator (Cornerstone 620 Oriel Newport Oriel Inc.) was used as a light source. A 10 nm slit assembly was used to obtain high optical power without sacrificing resolution. The output light from the monochromator was directed into an integrating sphere at the output of which the chip was mounted. The detector was reset for 2 ms and the integration time varied depending on the optical power. The integrated photocurrent was collected for wavelengths ranging from 330 to 800 nm in increments of 10 nm. The optical power of the incident beam was measured with an optical power meter (Newport Inc. model 1830-C).

To determine the spectral responsivity, the detector was reset 50 times at intervals corresponding to the chosen integration times. The slope of the average signal was calculated through a linear fit and normalized by the effective incident power. Figure 6 shows the spectral responsivity of the detector in both single-ended and differential mode, as well as the spectral responsivity of the detector in differential mode when a macroscopic emission filter (Chroma Corp. 60691) was placed

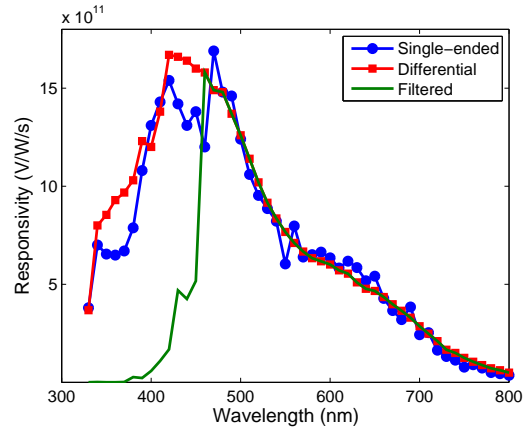


Fig. 6. Spectral responsivity in differential and single-ended modes, and in differential mode with a macroscopic emission filter

in between the integrating sphere and the chip. The detector has the same responsivity spectrum when operated in single-ended or in differential mode. When the emission filter is used, the response is attenuated at wavelengths below 420 nm, which is consistent with the transmission characteristics of the filter.

IV. FLUORESCENCE SENSING OF FURA-2 AND CALCIUM LEVEL MEASUREMENTS

Fura-2 is a widely used calcium ion Ca^{2+} indicator developed by Tsien et al. [7]. It has a large Stokes shift with emission intensity at 510 nm occurring for excitation wavelengths of 340 and 380 nm. The two excitation wavelengths allow ratiometric measurement which reduces the confounding effects of Fura-2 concentration, optical path distortions and photobleaching. Fura-2 is very stable and can be monitored for as long as an hour without significant loss of fluorescence from either leakage or bleaching. An illumination source (Newport Apex) and monochromator (Cornerstone 260 1/4m) were used to generate light at 340 nm and 380 nm. A cuvette holding the fluorophore was placed in a custom fixture that allowed it to be in close proximity to the emission filter (long pass filter with cut-on at 420 nm), and the sensor was placed on the other side of the filter. Since the dye itself is fluorescent we used this test fixture to first ascertain the sensitivity of the detector to Fura-2 concentration before determining the accuracy of the sensor using a calibration kit. In all cases the environmental illumination is first measured and subsequently subtracted from measured signals. The Fura-2 dye (in salt form) and calcium calibration buffer kit were obtained from Invitrogen.

To measure the sensitivity of the detector to Fura-2, a solution of the dye was prepared in Hanks Balanced Salt Solution (HBSS) free of Ca and EGTA at 1 mM concentration in 2 mL of HBSS. The solution was excited at 340 and 380 nm and the output of the sensor recorded with an integration time of 1 s. The concentration was then halved with care being taken to titrate a number of times to homogenize the solution. The output sensor voltage varies linearly with concentration

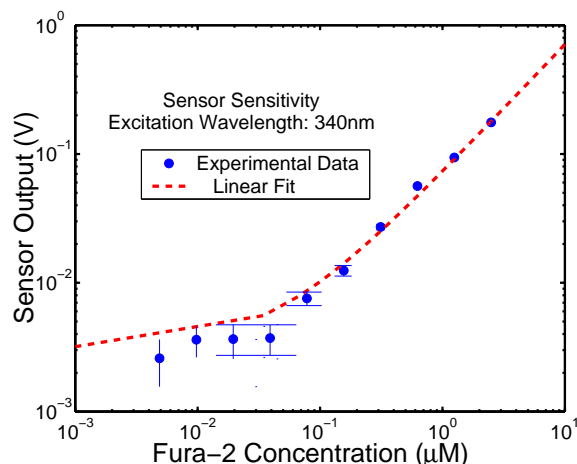


Fig. 7. Sensor output voltage as a function of Fura-2 concentration

(Fig 7). Concentrations as low as 39 nM were accurately measured. Error bars are included for all data but in some cases are too small to be visible.

As mentioned previously Fura-2 emits at 510 nm when excited by two different excitation wavelengths. For excitation at 340 nm the fluorescence intensity increases with increasing free Ca^{2+} concentration while at 380 nm the emission intensity decreases with increasing free Ca^{2+} concentration. This makes it possible to perform ratiometric measurements using Fura-2. A solution of the dye was prepared at 1 mM concentration. There were 11 buffer calibration solutions ranging from 0 to 39 μM free Ca^{2+} . Ten μL of Fura-2 was added to 2 mL of each buffer solutions to obtain a final concentration of 5 μM . Each was then excited at 340 nm and 380 nm, and sensor response to emission was observed with an integration time of 0.5 s. The Ca^{2+} concentration is related to the intensities by

$$[Ca^{2+}] = k_d \alpha = k_d \frac{R - R_{min} F_{max}^{380}}{R_{max} - R F_{min}^{380}} \quad (5)$$

where k_d is the dissociation constant, R is the ratio of the fluorescent intensity at 340 nm compared to 380 nm, R_{max} and R_{min} are the maximum and minimum ratios and F_{max}^{380} and F_{min}^{380} are the maximum and minimum sensor response at 380 nm. From the log-log plot of α vs Ca^{2+} shown in Fig 8, the dissociation constant is found to be 199 nM (previous published data from Invitrogen shows 145 nM) [7]. We reliably detected a free calcium concentration as low as 17 nM.

V. CONCLUSIONS

We presented a novel low noise sensor with differential readout using in-pixel sample and hold for fluorescence detection. This structure showed an improvement in reset noise and an improvement in readout noise over a comparable single-ended sensor by 1.42X and 9.20X respectively. The spectral responsivity was characterized and verified over near-UV and visible wavelengths. The sensor in conjunction with an external emission filter was used to demonstrate fluorescence detection and showed detection of Fura-2 concentration as low

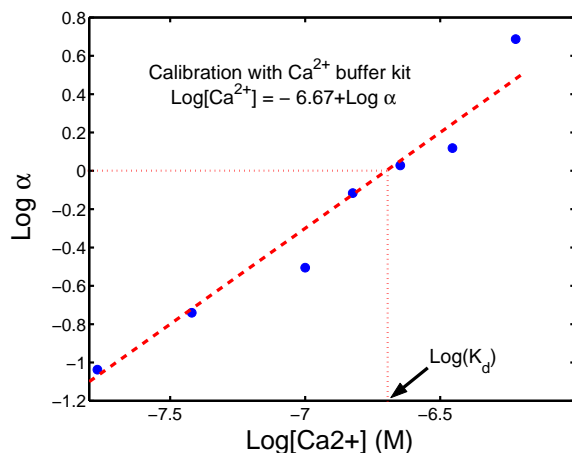


Fig. 8. Sensor output voltage as a function of $[Ca^{2+}]$

as 39 nM. The detection limit for Ca^{2+} using ratiometric measurement with Fura-2 was less than 17 nM.

VI. ACKNOWLEDGMENT

We would like to thank our colleagues from the Integrated Biomorphic Information Systems Laboratory for helpful discussions. We would also like to thank MOSIS for chip fabrication. These chips will be used to teach an undergraduate course in mixed-signal VLSI design. We are grateful to Jay Pyle for machining several of our test fixtures. The material is based upon work supported by the National Science Foundation under grants 0226589, 0238061, and 0515873. and by the Laboratory for Physical Sciences.

REFERENCES

- [1] M. A. Burns, B. N. Johnson, S. N. Brahmasandra, K. Handique, J. R. Webster, M. Krishnan, T. S. Sammarco, P. M. Man, D. Jones, D. Heldsinger, C. H. Mastrangelo, and D. T. Burke, "An integrated nanoliter DNA analysis device," *Science*, vol. 282, pp. 484-487, 1998.
- [2] O. Hofmann, X. H. Wang, J. C. deMello, D. D. C. Bradley, and A. J. deMello, "Towards microalbuminuria determination on a disposable diagnostic microchip with integrated fluorescence detection based on thin-film organic light emitting diodes," *Lab Chip*, vol. 5, pp. 863-868, 2005.
- [3] E. Thrush, O. Levi, W. Ha, K. Wang, S. J. Smith, and J. S. Harris, "Integrated bio-fluorescence sensor," *J. Chromatogr. A*, vol. 1013, pp. 103-110, 2003.
- [4] M. L. Chabinye, D. T. Chiu, J. C. McDonald, A. D. Stroock, J. F. Christian, A. M. Karger, and G. M. Whitesides, "An integrated fluorescence detection system in poly(dimethylsiloxane) for microfluidic applications," *Anal. Chem.*, vol. 73, pp. 4491-4498, 2001.
- [5] J. A. Chediak, Z. S. Luo, J. G. Seo, N. Cheung, L. P. Lee, and T. D. Sands, "Heterogeneous integration of CdS filters with GaN LEDs for fluorescence detection microsystems," *Sens. Actuator A-Phys.*, vol. 111, pp. 1-7, 2004.
- [6] B. Fowler, A. El Gamal, D.X.D Yang, and H. Tian, "A method for estimating quantum efficiency for CMOS image sensors," *Proceedings of SPIE*, 3301:178-185, 1998.
- [7] Invitrogen Corporation, "Fura and Indo Ratiometric Calcium Indicators," <http://www.invitrogen.com>, Product Notes, 2006.